

# Effect of the finite speed of light in ionization of extended systems

I. A. Ivanov<sup>1,\*</sup>, Anatoli S. Kheifets<sup>2</sup>, Kyung Taec Kim<sup>1,3</sup>

<sup>1</sup>*Center for Relativistic Laser Science, Institute for Basic Science, Gwangju 61005, Korea*

<sup>2</sup>*Research School of Physics, The Australian National University, Canberra ACT 2601, Australia*

<sup>3</sup>*Department of Physics and Photon Science, GIST, Gwangju 61005, Korea*

(Dated: July 14, 2021)

We study propagation effects due to the finite speed of light in ionization of extended systems. We present a general quantitative theory of these effects and show under which conditions such effects should appear. The finite speed of light propagation effects are encoded in the non-dipole terms of the time-dependent Schrödinger equation and display themselves in the photoelectron momentum distribution projected on the molecular axis. Our numerical modeling for the  $\text{H}_2^+$  molecular ion and the  $\text{Ne}_2$  dimer shows that the finite light propagation time from one atomic center to another can be accurately determined in a table top laser experiment which is much more readily affordable than an earlier synchrotron measurement by Grundmann *et al* [Science 370, 339 (2020)].

PACS numbers: 32.80.Rm 32.80.Fb 42.50.Hz

Every quantum system evolves on its characteristic time scale which varies widely between molecules (femtoseconds –  $10^{-15}$  s) [1], atoms (attoseconds –  $10^{-18}$  s) [2] and nuclei (zeptoseconds –  $10^{-21}$  s) [3]. A crossover between these time scales is very rare in nature. It was therefore quite unexpected to discover an ionization process in the hydrogen molecule that evolved on a zeptosecond time scale [4]. An explanation of this phenomenon appeared to be quite simple. While it takes tens of attoseconds for an electron to trespass the  $\text{H}_2$  molecule, the incoming light wave sweeps from one molecular end to another orders of magnitude faster. This results in one of the constituent hydrogen atoms getting ionized a fraction of the attosecond sooner than its counterpart. Such a tiny ionization delay manifests itself quite noticeably in the two-slit electron interference that the  $\text{H}_2$  molecule readily displays [5]. To discover a zeptosecond delay in molecular photoionization, Grundmann *et al.* [4] needed to deploy an extremely bright synchrotron source of highly energetic photons [6]. We demonstrate that even a table top laser experiment is capable of detecting a similar effect making it much more readily affordable.

In this Letter we present a general quantitative theory of the delay due to the finite speed of light propagation and we show under which conditions such effects should manifest themselves. In our numerical demonstrations, we consider the  $\text{H}_2^+$  molecular ion and the  $\text{Ne}_2$  dimer. The  $\text{H}_2^+$  molecular ion has been scrutinized since the early days of quantum mechanics [7] and was recently used as a model for the study of the interference effects in photon-momentum transfer for the process of molecular photoionization [8]. Photoionization studies of  $\text{Ne}_2$  is a novelty [9]. We subject both targets to an attosecond laser pulse that can be readily produced in high-order harmonics generation sources [10, 11]. The photoelectron flux encodes the timing information about the

ionization process. This flux is reconstructed by solving the laser-driven time-dependent Schrödinger equation (TDSE). The numerical results obtained for  $\text{H}_2^+$  using the TDSE can be interpreted in a transparent qualitative way by considering a very simple heuristic tight-binding model (TBM). This gives us a tool for understanding the time delay caused by the finite speed of light propagation. We apply this tool to  $\text{H}_2^+$  and  $\text{Ne}_2$  and find the time delay of a fraction of attosecond that depends sensitively on the orientation of the molecular axis relative to the propagation and polarization directions.

Our approach is based on the numerical solution of the three-dimensional TDSE

$$i\partial\Psi(\mathbf{r},t)/\partial t = [\hat{H}_{\text{mol}} + \hat{H}_{\text{int}}(t)]\Psi(\mathbf{r},t), \quad (1)$$

where  $\hat{H}_{\text{mol}}$  is the field-free one-electron Hamiltonian and  $\hat{H}_{\text{int}}(t)$  describes the field-target interaction. We consider a traveling wave propagating in the positive  $x$ -direction and polarized in the  $z$ -direction, described by the vector potential  $\mathbf{A}(t - x/c)$  with  $c = 137.036$  being the speed of light in atomic unites (a.u.).

We apply the procedure previously used in [12] to study non-dipole effects in atomic photoionization. The leading order relativistic corrections to  $\hat{H}_{\text{int}}(t)$  come from the linear term of the expansion of  $\mathbf{A}(t - x/c)$  in powers of  $c^{-1}$ . We plug this expansion into the standard minimal coupling Hamiltonian [13]  $\hat{H}_{\text{min}} = (\hat{\mathbf{p}} + \mathbf{e}_z A(x, t))^2/2$  and keep the terms linear in  $c^{-1}$ :

$$\hat{H}_{\text{int}}(\mathbf{r}, t) = \hat{p}_z A(t) + \frac{\hat{p}_x E(t)}{c} + \frac{A(t)E(t)x}{c} + \frac{A^2(t)}{2}. \quad (2)$$

In the above expression,  $A(t)$  no longer depends on the coordinates and  $E(t) = -\partial A(t)/\partial t$  is the electric field of the pulse. The last term on the r.h.s. of Eq. (2) is a function of time only and can, therefore, be removed by a unitary transformation. The interaction Hamiltonian (2) can be related by a gauge transformation to the Kramers-Henneberger Hamiltonian used in [14].

An additional source of relativistic corrections in  $\hat{H}_{\text{int}}$  is the interaction of the magnetic field of the pulse with

\*Electronic address: igorivanov@ibs.re.kr

the electron spin. These corrections cannot be obtained by a simple generalization of the minimal coupling Hamiltonian. To obtain them, one needs to consider systematically the transition of the Dirac equation to the non-relativistic limit [15]. The inclusion of the electron spin, however, is not necessary for the present study where we keep only the  $c^{-1}$  terms as was done, for instance, in [12, 16]. The Breit-Pauli relativistic corrections to  $\hat{H}_{\text{mol}}$ , such as the effects of the relativistic kinematics, spin-orbit interaction and the so-called Darwin term, are all of the order of  $c^{-2}$  [13] and can also be safely omitted.

The target interacts with a short laser pulse

$$A(t) = -E_0\omega^{-1} \sin^2(\pi t/T_1) \sin \omega t, \quad (3)$$

of the total duration  $T_1 = 4T$  with  $T = 2\pi/\omega$  and the base laser frequency  $\omega = 4.04$  a.u. (the photon energy of 110 eV). The peak electric field strength  $E_0 = 0.1$  au corresponds to the intensity of  $3.5 \times 10^{14}$  W/cm<sup>2</sup>

To solve the TDSE (1) we follow the procedure that we employed previously in the non-relativistic case [17–19]. A solution of the TDSE is sought in the spherical coordinates as an expansion over the spherical harmonics basis

$$\Psi(\mathbf{r}, t) = \sum_{l,m}^{l_{\text{max}}} f_{lm}(r, t) Y_{lm}(\hat{r}), \quad (4)$$

The radial grid is discretized with the step  $\delta r = 0.05$  a.u. in a box of the size  $R_{\text{max}} = 400$  au which, together with  $l_{\text{max}} = 10$ , ensured a numerical convergence. We characterize the final photoelectron state by its asymptotic momentum  $\mathbf{p}$ . Ionization amplitudes  $a_{\mathbf{p}}$  are obtained by projecting the TDSE solution after the end of the pulse on the ingoing scattering states  $\phi_{\mathbf{p}}^-$  [20].

For a weak electromagnetic field that we employ, we can also obtain an analytical expression for the ionization amplitude by using the perturbation theory (PT) formula and treating the operator (2) as a perturbation:

$$a_{\mathbf{p}} = -i \int_{-\infty}^{+\infty} \langle \phi_{\mathbf{p}}^- | \hat{H}_{\text{int}}(\tau) | \phi_0 \rangle e^{i(E_{\mathbf{p}} - \varepsilon_0)\tau} d\tau. \quad (5)$$

Here  $\phi_0$  and  $\phi_{\mathbf{p}}^-$  are the initial and final molecular states with the corresponding energies  $\varepsilon_0$  and  $E_{\mathbf{p}}$ .

We split the ionization amplitude (5)  $a_{\mathbf{p}} = a_{\mathbf{p}}^{(0)} + a_{\mathbf{p}}^{(1)}$  into the nonrelativistic part  $a_{\mathbf{p}}^{(0)}$  and the first order relativistic correction  $a_{\mathbf{p}}^{(1)}$ . By introducing the Fourier transforms  $A(t) = (2\pi)^{-1} \int a(\Omega) e^{-it\Omega} d\Omega$  and  $A^2(t) = (2\pi)^{-1} \int b(\Omega) e^{-it\Omega} d\Omega$  we obtain for these amplitudes:

$$a_{\mathbf{p}}^{(0)} = -ia(\Omega) \langle \phi_{\mathbf{p}}^- | \hat{p}_z | \phi_0 \rangle, \quad \Omega = E_{\mathbf{p}} - \varepsilon_0 \quad (6)$$

$$\begin{aligned} a_{\mathbf{p}}^{(1)} &= \Omega c^{-1} (a(\Omega) \langle \phi_{\mathbf{p}}^- | \hat{p}_z x | \phi_0 \rangle + b(\Omega) \langle \phi_{\mathbf{p}}^- | x | \phi_0 \rangle / 2) \\ &\approx \Omega c^{-1} a(\Omega) \langle \phi_{\mathbf{p}}^- | \hat{p}_z x | \phi_0 \rangle. \end{aligned} \quad (7)$$

The second term on the right hand side of Eq. (7) can be neglected because the ratio of the second term and the first term in this expression is approximately  $b(\Omega)/(a(\Omega)p)$ , where  $p$  is the typical value of the momentum of the ionized electron. For the pulse parameters that we consider, this value can be estimated as  $E_0/(\omega p) \approx 0.01$ .

It can be seen from Eq. (7) that the relativistic correction  $a_{\mathbf{p}}^{(1)}$  vanishes in certain cases. In particular, it is zero for an axially symmetric system with the field-free Hamiltonian that is invariant under rotations about the  $z$ -axis. Indeed, for such systems the scattering state  $\phi_{\mathbf{p}}^-(\mathbf{r})$  is a function of the arguments  $z, p_z, \rho, p_\rho$  and  $\boldsymbol{\rho} \cdot \mathbf{p}_\rho$ , where  $z, p_z$  and  $\boldsymbol{\rho}, \mathbf{p}_\rho$  are the components of the  $\mathbf{r}$  and  $\mathbf{p}$  vectors parallel and perpendicular, respectively, to the  $z$ -axis of the coordinate system that we employ. For an axially symmetric system the ground state wave function  $\phi_0$  in Eq. (7) (which we assume to be non-degenerate) is invariant under rotations about the  $z$ -axis. We obtain then from Eq. (7):  $a^{(1)}(p_x, p_y, p_z) = -a^{(1)}(-p_x, p_y, p_z)$ . Therefore the amplitude  $a_{\mathbf{p}}^{(1)}$  is zero in the plane  $p_x = 0$  which encompasses the most important region of the momenta near the maximum of the momentum distribution.

The effect of the propagation correction (7) can be most easily illustrated within the tight-binding model in which the ground state of  $\text{H}_2^+$  and  $\text{Ne}_2$  is represented by a Heitler-London wave function

$$\phi_0(\mathbf{r}) = [\phi(\mathbf{r} - \mathbf{R}/2) + \phi(\mathbf{r} + \mathbf{R}/2)]/\sqrt{2}.$$

In the TBM, the overlap of the two terms is small and  $\phi(\mathbf{r})$  is represented by a spherically symmetric atomic-like state. Under these conditions, and by employing the Born approximation for the scattering state  $\phi_{\mathbf{p}}^-$ , which is justified for the relatively high electron energies considered here, we obtain:

$$a_{\mathbf{p}}^{(0)} = a_d(\mathbf{p}) \sqrt{2} \cos(\mathbf{p} \cdot \mathbf{R}/2), \quad (8)$$

$$a_d(\mathbf{p}) = -ia(\Omega) \langle \mathbf{p} | \hat{p}_z | \phi \rangle \quad (9)$$

$$a_{\mathbf{p}}^{(1)} = -\Omega c^{-1} (\partial/\partial p_x) a_{\mathbf{p}}^{(0)}. \quad (10)$$

The non-relativistic term  $a_{\mathbf{p}}^{(0)}$  is represented by the single-center dipole amplitude (9) modulated by the two-center interference factor [5]. Adding the relativistic term leads to

$$a_{\mathbf{p}} = a_{\mathbf{p}}^{(0)} + a_{\mathbf{p}}^{(1)} \approx a_d(\mathbf{p}) \sqrt{2} \cos(\mathbf{p} \cdot \mathbf{R}/2 + \delta), \quad (11)$$

where  $\delta = -\boldsymbol{\kappa} \cdot \mathbf{R}/2$  and  $\boldsymbol{\kappa} = \Omega c^{-1} \mathbf{e}_x$  is the photon momentum. It is this phase factor  $\delta$  that is responsible for the modified interference pattern observed and decoded in [4].

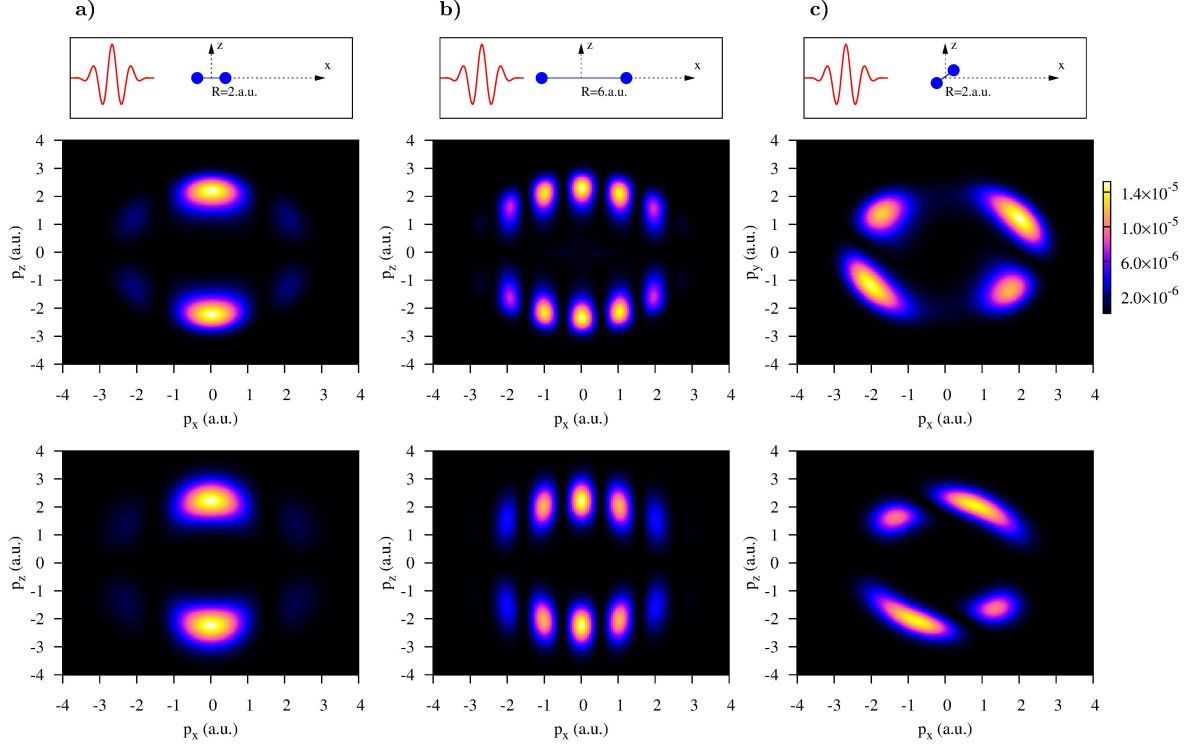


FIG. 1: (Color online) The photoelectron momentum distributions projected on the  $(p_x, p_y)$ -plane for different orientations and inter-nuclear distances of  $\text{H}_2^+$  illustrated in the top row of panels. The middle row of panels displays the numerical TDSE results while the bottom row exhibits the corresponding TBM results obtained using Eq. (8).

Appearance of the additional phase factor  $\delta$  in Eq. (11) is due to an extra propagation time of the light wave from one end of the molecule to the other. This interpretation becomes yet more transparent if we use coordinate representation for the part of the wave-function describing the ionized wave packet:

$$\Psi_{\text{ion}}(\mathbf{r}, t) = \int a_{\mathbf{p}} \phi_{\mathbf{p}}^-(\mathbf{r}) e^{-iE_{\mathbf{p}}t} d\mathbf{p}, \quad (12)$$

where  $\phi_{\mathbf{p}}^-(\mathbf{r})$  are the molecular scattering states. To evaluate this integral in the limit  $t \rightarrow \infty$ , we rely on the saddle-point method (SPM) that is commonly used in description of ionization [21, 22] or scattering [23] processes. By writing  $a_d(\mathbf{p}) = |a_d(\mathbf{p})|e^{i\eta(\mathbf{p})}$  in Eq. (11) and employing the SPM, we obtain from Eq. (12):

$$\lim_{t \rightarrow \infty} \Psi_{\text{ion}}(\mathbf{r}, t) = e^{i\mathbf{p}_m \cdot \mathbf{r}} \left\{ G[\mathbf{r} + \mathbf{R}/2 - \mathbf{p}_m(t - \tau - \tau_1)] + G[\mathbf{r} - \mathbf{R}/2 - \mathbf{p}_m(t - \tau + \tau_1)] \right\}. \quad (13)$$

Here  $\mathbf{p}_m$  is the most probable photoelectron momentum,  $\tau = \partial\eta/\partial E$  is the usual Wigner photoemission time-delay [24] and  $\tau_1 = \partial\delta/\partial E = -R_x/(2c)$  with  $\delta = -\kappa \cdot \mathbf{R}/2$  from Eq. (11).

The  $\tau_1$  term represents an additional time that it takes for the light pulse to cover the distance  $R_x = \mathbf{R} \cdot \mathbf{e}_x$ .

The wave packet  $G(\mathbf{r})$  in Eq. (13) is a Fourier transform of the dipole amplitude  $a_d(\mathbf{p})$  in Eq. (11). Importantly,  $G(\mathbf{r})$  has a strong peak near the origin. Therefore the two terms in Eq. (13) describe two wave packets emitted from the two atomic centers  $\mathbf{r} = -\mathbf{R}/2$  and  $\mathbf{r} = \mathbf{R}/2$  at the times  $\tau + \tau_1$  and  $\tau - \tau_1$ , respectively. For transparency of derivation, we omitted in Eq. (13) the Coulomb terms which would only add slowly varying (logarithmic) corrections in the arguments of  $G(\mathbf{r})$  [21, 22]. These additional logarithmic terms are the same for the two wave packets and they would therefore cancel in the time delay difference between these wave packets.

We note that the right-hand side of Eq. (9) can be represented as a product of two factors, the factor  $p_z$  responsible for the angular dependence of the amplitude and the Gaussian factor  $\exp\{-a(p - p_0)^2\}$  representing the energy conservation  $p_0^2/2 = \varepsilon_0 + \omega$ . Such a Gaussian representation of the ionized wave packets emitted in the single-center problems is often used in studying temporal dynamics of atomic ionization [21, 22]. The parameter  $a$  determines the width of the wave packet and depends on the pulse parameters. One can derive an analytical expression for its value but we will not need it in the following. By employing the Gaussian ansatz for  $a_d(\mathbf{p})$

and Eq. (11) we finally obtain

$$a_{\mathbf{p}} = A \exp \left\{ -a(p - p_0)^2 \right\} p_z \cos(\mathbf{p} \cdot \mathbf{R}/2 + \delta). \quad (14)$$

We use Eq. (14) to evaluate the photoelectron emission pattern and to compare it with the fully *ab initio* TDSE calculations for various orientations and different internuclear distances of  $\text{H}_2^+$ . This comparison is presented in Figure 1. The top row of panels illustrates the geometry of the ionization process. It is assumed that the molecular axis is confined to the  $xz$ -plane where the propagation and polarization vectors of the pulse belong, making an angle  $\theta$  with the propagation direction. In (a-b),  $\theta = 0$  while in (c)  $\theta = \pi/4$ . The photoelectron momentum distribution is projected on the  $xz$  plane and computed as  $P(p_x, p_z) = \int |a_{\mathbf{p}}|^2 dp_y$  with the amplitude  $a_{\mathbf{p}}$  obtained by projecting the TDSE solution on the set of the scattering states of  $\text{H}_2^+$ . The number and location of the bright spots in Figure 1 reflect a simple two-center interference pattern governed by the cosine term in Eq. (14).

Comparison of the TDSE calculations (the middle row of panels in Figure 1) and results based on Eq. (14) (the bottom row of panels) shows that the TBM reproduces the spectra very well for the geometries that we consider. We will, therefore, analyze and interpret our TDSE results using this transparent model that is equally applicable to both  $\text{H}_2^+$  and  $\text{Ne}_2$ . We will focus on the photoelectron momentum distribution projected on the  $(xz)$  plane and integrated over the momentum component  $p_{\perp}$  which is perpendicular to the molecular axis. Such a momentum distribution is a function of the momentum component  $p_{\parallel}$  which is parallel to the molecular axis. By employing the Gaussian ansatz (14) we obtain:

$$P(p_{\parallel}) = \int P(\mathbf{p}) dp_y dp_{\perp} \quad (15)$$

$$\approx B \exp \left\{ -C p_{\parallel}^2 \right\} \cos^2 \left( \frac{p_{\parallel} R}{2} + \delta \right).$$

We use the analytical expression (15) with adjustable parameters  $B$ ,  $C$  and  $\delta$  to fit  $P(p_{\parallel})$  obtained from the numerical TDSE calculations. The accuracy of the fitting procedure is illustrated in Figure 2a) and b) where we display  $P(p_{\parallel})$  for the two geometries illustrated in Figure 1a) and b), respectively. In both cases,  $\theta = 0$  and  $P(p_{\parallel})$  is simply the projection of the 2D momentum distribution on the horizontal axis. As is seen in Figure 2, the analytical fit with Eq. (15) represents the TDSE calculation with the corresponding  $R$  value quite accurately. This allows us to extract the phase shift  $\delta$  accumulated due to the finite speed of light propagation.

In Figure 3 we display thus extracted phase shifts  $\delta$  for the three molecular orientations illustrated in Figure 1. To enhance the relativistic effects, we artificially decrease the speed of light from its physical value  $c = c_0 = 137.036$  a.u. down to  $c = c_0/10$ . According to TBM, the phase shift should scale linearly as  $\delta = \alpha c_0/c$  with the slope  $\alpha = -R_x \kappa/2$ . The predicted linear scaling is confirmed very accurately by the numerical values

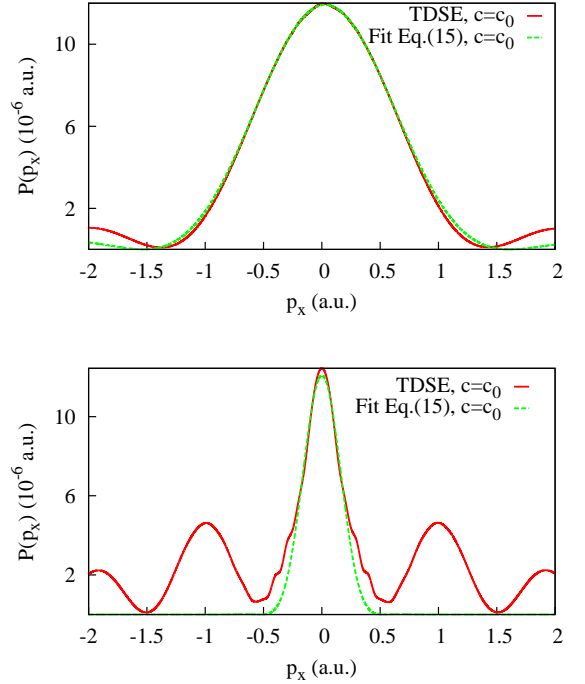


FIG. 2: (Color online) The photoelectron momentum distribution projected on the molecular axis for geometries illustrated in Figure 1a) (top) and 1b) (bottom). The fit based on Eq. (15) and TDSE calculations are plotted with the solid and dotted lines, respectively.

TABLE I: Propagation delay for different geometries and internuclear distances.

R (a.u.)	$\theta$	Fit (as)	$R_x/c$ (as)
2	0	0.46	0.35
2	$\pi/4$	0.17	0.24
6	0	1.56	1.05

shown in Figure 3 with only a small error margin. The time delay values corresponding to the physical speed of light  $c_0$  are shown in Table I in comparison with the estimate  $\Delta t = 2R_x/c_0$  provided by the TBM. Agreement of the results can be deemed quite satisfactory given the relative simplicity of TBM. More importantly, the linear dependence of the TDSE results on the parameter  $c_0/c$  clearly demonstrates existence of the finite speed of light effect in ionization of diatomic molecules.

In conclusion, our work was motivated by the synchrotron based experiment by Grundmann et al. [4] who discovered a zeptosecond time delay in photoionization of the  $\text{H}_2$  molecule. We aimed to demonstrate that a similar delay, which is caused by the finite speed of light propagation from one constituent atom to another, can be detected in a much more accessible table top laser settings. In doing so, we developed a general theory of the finite speed of light propagation effects in ionization of extended systems. As a simple case study, we considered the  $\text{H}_2^+$  molecular ion interacting with a short

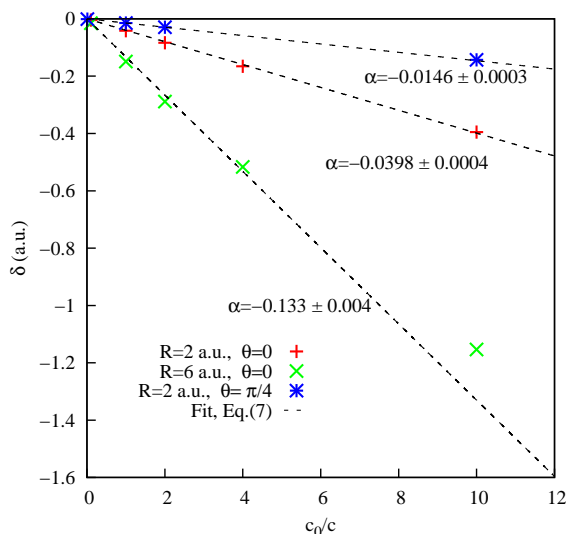


FIG. 3: (Color online) Parameter  $\delta$  in Eq. (15) for different geometries and internuclear distances.

laser pulse. This target affords a very accurate numerical treatment within the time-dependent Schrödinger equation. At the same time, an heuristic tight-binding model employing the Heitler-London molecular ground state produces very similar results. TBM can be easily adopted to the  $\text{Ne}_2$  dimer by a simple increase of the inter-atomic distance to  $R \simeq 6$  a.u. Notably, the corre-

sponding interference pattern displayed in Figure 1b) is very similar to that obtained in the experiment [9] and the earlier SPM modeling [25].

Our simulations demonstrate that the speed of light delay in ionization of diatomic molecular targets can be decoded from the photoelectron momentum distribution projected on the molecular axis. This method has a clear advantage over the earlier synchrotron measurement based on decoding the 2D interference pattern [4]. Indeed, the bright interference spots have a finite angular width. To detect their shift due to the finite speed of light requires a sufficiently large photon momentum that should not be vanishingly small in comparison with the photoelectron momentum. This in turn requires very high photon energy (800 eV in [4]). Fitting of a one-dimensional momentum distribution produces significantly reduced error bars. Thus smaller values of the photon momentum and energy can be used (100 eV in our simulations). In addition, by projecting the momentum distribution on the molecular axis, we increase the count rate and improve statistics of the measurement. Hence the photon flux can be significantly reduced. This reduction of both the photon flux and energy makes the proposed method much more readily accessible in desk-top conventional laser settings. This we hope will stimulate further speed of light delay determinations in diatomic molecules and other extended systems.

- 
- [1] F. Remacle and R. D. Levine, *An electronic time scale in chemistry*, Proc. Nat. Acad. Sci. **103**(18), 6793 (2006).
  - [2] F. Krausz and M. Ivanov, *Attosecond physics*, Rev. Mod. Phys. **81**, 163 (2009).
  - [3] A. E. Kaplan and P. L. Shkolnikov, *Lasotron: A proposed source of powerful nuclear-time-scale electromagnetic bursts*, Phys. Rev. Lett. **88**, 074801 (2002).
  - [4] S. Grundmann, D. Trabert, K. Fehre, N. Strenger, A. Pier, L. Kaiser, M. Kircher, M. Weller, S. Eckart, L. P. H. Schmidt, et al., *Zeptosecond birth time delay in molecular photoionization*, Science **370**, 339 (2020).
  - [5] H. D. Cohen and U. Fano, *Interference in the photoionization of molecules*, Phys. Rep. **150**(1), 30 (1966).
  - [6] J. Viehhaus, F. Scholz, S. Deinert, L. Glaser, M. Ilchen, J. Seltmann, P. Walter, and F. Siewert, *The Variable Polarization XUV Beamline P04 at PETRA III : Optics, mechanics and their performance*, Nucl. Instrum. Methods Phys. Res. A **710**, 151 (2013).
  - [7] L. Pauling, *The application of the quantum mechanics to the structure of the hydrogen molecule and hydrogen molecule-ion and to related problems.*, Chemical Reviews **5**(2), 173 (1928).
  - [8] S. Chelkowski and A. D. Bandrauk, *Photon-momentum transfer in molecular photoionization*, Phys. Rev. A **97**, 053401 (2018).
  - [9] M. Kunitski, N. Eicke, P. Huber, J. Köhler, S. Zeller, J. Voigtsberger, N. Schlott, K. Henrichs, H. Sann, F. Trinter, et al., *Double-slit photoelectron interference in strong-field ionization of the neon dimer*, Nature Com-
  - [10] S. L. Cousin, N. Di Palo, B. Buades, S. M. Teichmann, M. Reduzzi, M. Devetta, A. Kheifets, G. Sansone, and J. Biegert, *Attosecond streaking in the water window: A new regime of attosecond pulse characterization*, Phys. Rev. X **7**, 041030 (2017).
  - [11] X. Ren, J. Li, Y. Yin, K. Zhao, A. Chew, Y. Wang, S. Hu, Y. Cheng, E. Cunningham, Y. Wu, et al., *Attosecond light sources in the water window*, Journal of Optics **20**(2), 023001 (2018).
  - [12] I. A. Ivanov, J. Dubau, and K. T. Kim, *Nondipole effects in strong-field ionization*, Phys. Rev. A **94**, 033405 (2016).
  - [13] I. I. Sobelman, *Introduction to the Theory of Atomic Spectra* (Pergamon Press, New York, 1972).
  - [14] M. Førre, Phys. Rev. A **74**, 065401 (2006).
  - [15] E. M. Lifshitz and V. B. Berestetskii, *Quantum Electrodynamics* (Pergamon Press, 1982).
  - [16] S. Chelkowski, A. D. Bandrauk, and P. B. Corkum, *Photon-momentum transfer in multiphoton ionization and in time-resolved holography with photoelectrons*, Phys. Rev. A **92**, 051401(R) (2015).
  - [17] I. A. Ivanov, *Evolution of the transverse photoelectron-momentum distribution for atomic ionization driven by a laser pulse with varying ellipticity*, Phys. Rev. A **90**, 013418 (2014).
  - [18] I. A. Ivanov and A. S. Kheifets, *Time delay in atomic photoionization with circularly polarized light*, Phys. Rev. A **87**, 033407 (2013).
  - [19] I. A. Ivanov and A. S. Kheifets, *Strong-field ionization of*

- he by elliptically polarized light in attoclock configuration*, Phys. Rev. A **89**, 021402 (2014).
- [20] L. D. Landau and E. M. Lifshitz, *Quantum Mechanics* (Pergamon Press, New York, 1977).
  - [21] A. S. Kheifets and I. A. Ivanov, *Delay in atomic photoionization*, Phys. Rev. Lett. **105**(23), 233002 (2010).
  - [22] I. A. Ivanov, *Double photoionization of the hydrogen molecule from the viewpoint of the time-delay theory*, Phys. Rev. A **86**, 023419 (2012).
  - [23] M. L. Goldberger and K. M. Watson, *Collision theory* (John Wiley and Sons, New York, 1964).
  - [24] E. P. Wigner, *Lower limit for the energy derivative of the scattering phase shift*, Phys. Rev. **98**, 145 (1955).
  - [25] V. V. Serov, A. W. Bray, and A. S. Kheifets, *Numerical attoclock on atomic and molecular hydrogen*, Phys. Rev. A **99**, 063428 (2019).